crystals

MDPI

Article

The Investigation of New Phosphate–Titanite Glasses According to Optical, Physical, and Shielding Properties

Khalid I. Hussein [1,2,*], Mohammed S. Alqahtani [1,3], Khloud J. Alzahrani [1], Heba Y. Zahran [4,5], Ali M. Alshehri [4], Ibrahim S. Yahia [4,5,6], Manuela Reben [7] and El Sayed Yousef [4,5]

1. Department of Radiological Sciences, College of Applied Medical Sciences, King Khalid University, Abha 61421, Saudi Arabia; mosalqhtani@kku.edu.sa (M.S.A.); 437808203@kku.edu.sa (K.J.A.)
2. Department of Medical Physics and Instrumentation, National Cancer Institute, University of Gezira, Wad Medani 2667, Sudan
3. BioImaging Unit, Space Research Centre, Department of Physics and Astronomy, University of Leicester, Leicester LE1 7RH, UK
4. Physics Department, Faculty of Science, King Khalid University, Abha 61413, Saudi Arabia; heldemardash@kku.edu.sa (H.Y.Z.); amshehri@kku.edu.sa (A.M.A.); ihussein@kku.edu.sa (I.S.Y.); ayousf@kku.edu.sa (E.S.Y.)
5. Research Center for Advanced Materials Science (RCAMS), King Khalid University, Abha 61413, Saudi Arabia
6. Nanoscience Laboratory for Environmental and Biomedical Applications (NLEBA), Semiconductor Laboratory, Department of Physics, Faculty of Education, Ain Shams University, Roxy, Cairo 11757, Egypt
7. Faculty of Materials Science and Ceramics, AGH–University of Science and Technology, Al. Mickiewicza 30, 30-059 Cracow, Poland; manuelar@agh.edu.pl

* Correspondence: kirahim@kku.edu.sa

Citation: Hussein, K.I.; Alqahtani, M.S.; Alzahrani, K.J.; Zahran, H.Y.; Alshehri, A.M.; Yahia, I.S.; Reben, M.; Yousef, E.S. The Investigation of New Phosphate–Titanite Glasses According to Optical, Physical, and Shielding Properties. *Crystals* **2022**, *12*, 941. https://doi.org/10.3390/cryst12070941

Academic Editors: Ana Pilar Valerga Puerta, Severo Raul Fernandez-Vidal, Zhao Zhang and Umberto Prisco

Received: 10 June 2022
Accepted: 1 July 2022
Published: 4 July 2022

Abstract: The melt-quenching approach was used to prepare phosphate–titanite glasses with the composition P_2O_5-Na_2O-CaO-8KF-$CaCl_2$-xTiO_2 (where x = 2, 4, and 6) in a mol %. The optical, physical, and shielding properties, such as the mass attenuation coefficient (MAC), half-value layer (HVL), effective electron density (N_{eff}), and effective atomic number (Z_{eff}), of the glasses were investigated at energies ranging between 15 and 200 keV. The shielding parameters were investigated using recently developed software (MIKE). The optical properties were examined using devices such as UV-Vis-NIR spectroscopy over wavelengths ranging between 190 and 2500 nm. The reported results showed that increasing the concentration of TiO_2 led to an increase in the density from 2.657 to 2.682 g/cm^3 and an increase in the OPD from 66.055 to 67.262 mol/L, while the molar volume (V_M) and oxygen molar volume (V_O) decreased from 39.21 to 39.101 cm^3/mol and from 15.139 to 14.867 cm^3/mol, respectively. The energy gap was found to decrease from 3.403 to 3.279 eV when the TiO_2 concentration increased. Furthermore, as the surface plasmon resonance of TiO_2 increases, so does its third-order susceptibility, non-linear refractive indices, linear attenuation, and mass attenuation. The shielding performance evaluation indicates that the most suitable energy range is between 15 and 50 keV. Based on the results, the PCKNT3 glass sample exhibits the highest attenuation performance of all of the samples tested.

Keywords: phosphate–titanite glasses; absorbance spectra; optical energy gap; third-order susceptibility; non-linear refractive indices; mass attenuation coefficient

1. Introduction

Metal oxides such as sodium oxide (Na_2O), calcium oxide (CaO), magnesium oxide (MgO), phosphorus pentoxide (P_2O_5), thallium oxide (TiO_2), and silicon dioxide (SiO_2) have been discovered to be necessary components for glass-ceramics and glasses, as well as bioactive glasses [1,2]. Their physical and optical performance factors, such as their refractive-index- or energy-gap-based oxide ion polarizability, cation polarizability, and optical basicity, make them suitable candidates for different optical applications [2]. A considerable contribution to the existing literature on advanced medical applications is made by theoretical investigations into bioactive glasses and their radiation attenuation capacities, which are difficult or impossible to accomplish experimentally or clinically. By delivering biomaterial-driven regenerative medicine, bioactive glasses enable the discovery of new techniques in medicine. This has cleared the path for bioactive glasses to be used as implant materials in medical repair and replacement procedures. Bioactive materials have been employed in a variety of applications, from dental to soft tissue healing. The first bioactive glass-ceramic created with the chemical form of 45 wt% SiO_2, 24.5 wt% CaO, 24.5 wt% Na_2O, and 6.0 wt% P_2O_5 [3] showed good biocompatibility and bone-bonding ability. This sample is known as 45S5 bio-glass. During therapeutic and diagnostic operations, bioactive materials can interact with ionizing radiation. Because bioactive glasses are used inside the human body for the aforementioned purposes, they may be subjected to harmful radiation from X-ray and gamma-ray equipment, which are commonly employed in hospitals to detect and cure disorders in the human body. Titanium dioxide has been widely investigated as an implant material in dental and orthopedic implants. Results show that it has good mechanical and biocompatibility compared to other existing materials such as stainless steel and cobalt–chrome alloys [4–7]. A complete understanding of photon interactions with various phosphate–titanite glass compositions, including their X-ray and gamma photon interactions, is therefore critical and must be achieved. Several studies have been conducted to evaluate the effectiveness of phosphate–titanite materials in shielding applications as well as their mechanical and optical properties [8–13]. Al-Harbi et al. (2020) studied the shielding characteristics of a glass system comprising phosphate glasses with the composition SiO_2–Na_2O–P_2O_5–CaO–B_2O_3 using MCNP5 and Phys-X software. Good radiation protection was reported at the low energies of 15 to 40 keV. Alalawi et al. (2020) studied the shielding effectiveness of phosphate glasses as bioactive glass systems with the structureP_2O_5-Na_2O-CaO-K_2O-MgO at nuclear medicine energies. Their results indicate that the addition of K_2O has a significant effect on shielding properties. Another factor that also should be considered is the radiation-induced point defects in oxides. Highly ionic MgO, partly covalent corundum (Al_2O_3), ferroelectric $KNbO_3$, silica-based optical fibers, fiber-based devices, and optical fiber sensors were reported [14,15]. This material, if irradiated by energetic particles, leads to the displacement of an atom into an interstitial position, leaving a vacancy behind. Most radiation shielding materials are made of lead, which has a high atomic number and high shielding efficiency. On the other hand, the lead is considered to be a toxic, heavy, and electron-contaminated material that increases the dose that staff and patients are exposed to, especially when dealing when equipment for patient contact shielding, such as protective lead aprons and thyroid shields placed in contact with a patient's skin to protect sensitive organs such as the chest, thyroid, and lenses of eyes. In this paper, we presented a new phosphate–titanite glass system with the composition $45P_2O_5$-20CaO-$15CaCl_2$-8KF-$10Na_2O$-$xTiO_2$ (where x = 2, 4, and 6), encoded by PCKNT1, PCKNT2, and PCKNT3 to replace the existing toxic shielding material used in dental and low-energy diagnostic applications. The shielding parameters include the linear attenuation coefficient (LAC), mass attenuation coefficient (MAC), half-value layer (HVL), mean free path (MFP), and effective atomic number (Z_{eff}). In addition, the optical and physical properties of the prepared glasses were studied at low energies to replace the toxic shielding materials and to reduce the amount of exposure doses.

2. Materials and Methods

2.1. Sample Preparation

Phosphate–titanite glasses with the composition $45P_2O_5$-20CaO-$15CaCl_2$-8KF-$10Na_2O$-$xTiO_2$ (where x = 2, 4, and 6) in a mol percentage were prepared using the melt-quenching technique. The raw materials were put in a Pt crucible in the heating furnace at a temperature in the range of 1200 to 1250 °C for 30 min, depending on the composition. The melt was stirred, and when the viscosity was high, the melt was cast in the brass mold. The prepared sample was put in the annealing furnace for 2 h at 420 °C, and after that, it was switched off. A helium pycnometer (UltraPyc1200e) was used to measure the sample densities. The sample densities and the chemical compositions of the prepared samples together with the computed refractive index (n) are illustrated in Table 1.

Table 1. The composition, density (ρ), and refractive index (n) of the PCKNT glass system.

Sample Code	Composition (mol%)	Density in $gcm^{-3} \pm 0.037$	Refractive Index
PCKNT1	$45P_2O_5$-20CaO-$15CaCl_2$-8KF-$10Na_2O$-$2TiO_2$	2.657	1.616
PCKNT2	$45P_2O_5$-20CaO-$15CaCl_2$-8KF-$10Na_2O$-$4TiO_2$	2.6792	1.637
PCKNT3	$45P_2O_5$-20CaO-$15CaCl_2$-8KF-$10Na_2O$-$6TiO_2$	2.6827	1.649

The radiation parameters were calculated using a recently developed software package, MIKE [16]. The shielding performance of the glass samples was evaluated and compared to other phosphate–titanite glasses materials that are reported in the literature.

2.2. Optical Properties

The average molar weight of the mixtures, $\overline{M}$, can be calculated from the mole fractions, x_i, of the constituent elements and their molar masses, M_i [17]:

$$\overline{M} = \sum x_i M_{i,} \tag{1}$$

where x_i is the element molar fraction, and M_i is the glassy composition molecular weight.

The change in the sample structure with respect to the molar composition can be better explained in terms of the molar volume rather than the density of the sample material, which expresses the oxygen distribution in the sample structure. The molar volume (V_M) of glass materials can be calculated using the following equation [17]:

$$V_M = \frac{\overline{M}}{\rho} \tag{2}$$

where M is the average molar weight of the sample and ρ is the density of the sample. The parameter that measured the volume of glass in 1 mole of oxygen is known as the oxygen molar volume V_O, which can be calculated using the following equation [17]:

$$V_O = V_M \left(\frac{1}{\sum x_i n_i} \right) \tag{3}$$

where V_M is the molar volume of the glass material, x_i is a molar fraction, and n_i is the number of oxygen atoms in each oxide.

The oxygen packing density (OPD) of any glass material that characterizes the optical properties of the glass samples can be calculated using the following relationship [17]:

$$OPD = 1000 \sum x_i n_i \left(\frac{1}{V_M} \right) \tag{4}$$

where V_M is the molar volume of the glass materials, x_i is a molar fraction, and n_i is the number of oxygen atoms in each oxide.

The molar refraction (R_m) can be calculated using the following equation [17]:

$$R_m = \frac{n^2 - 1}{n^2 + 2} \times V_M \tag{5}$$

The reflection loss, R_L in percentage, can be calculated using the following equation [17]:

$$R_L = \left[\frac{(n-1)}{(n+1)} \right]^2 \tag{6}$$

where n is the refractive index of the glass materials.

The molar electronic polarizability (α_m) can be calculated using the following equation [17]:

$$\alpha_m = \frac{R_m}{2.52} \tag{7}$$

The Miller coefficient estimated to determine the first-order nonlinear optical susceptibility of the isotropic medium, χ^1, can be computed as follows: $\chi^{(1)} = \frac{(n^2-1)}{4\pi}$; the third-order nonlinear optical susceptibility, $\chi^{(3)}$, can be determined by $\chi^{(3)} = 1.7 \times 10^{-10}\left[\chi^{(1)}\right]^4$ esu; and the nonlinear refractive indices, n_2, are calculated according to $n_2 = \frac{12\pi\chi^{(3)}}{n}$.

2.3. Shielding Properties

When a mono-energetic photon beam with an initial intensity of I_0 travels through a d cm thick barrier, its intensity is reduced according to the Beer–Lambert law [18]:

$$\text{LAC} = \mu = -\frac{\ln\frac{I}{I_0}}{d} \tag{8}$$

where I_0, I, and μ represent the un-attenuated and attenuated photon intensity, and the linear attenuation coefficient, respectively.

On the other hand, the mass attenuation coefficient, μ_m =(μ/ρ), is defined as the probability of photons interacting within the barrier and can be calculated using the following equation [19]:

$$\text{MAC} = \frac{\mu}{\rho} = \sum wi\left(\frac{\mu}{\rho}\right)_i \tag{9}$$

where $(wi,\ (\mu/\rho)_i\ (cm^2/g),\ \rho)$ represents the fractional weight and the mass attenuation coefficient of the individual components in each component, and ρ indicates the density of the material, respectively.

The total atom cross section (σ_a) and total electronic cross section (σ_e), which characterize the probability of photon interaction within the material, can be calculated using the following relationships [19,20]:

$$\sigma_a = \sigma_m \frac{1}{\sum i\, n_i} = \frac{(\mu/\rho)_{target}}{N_A \sum i \frac{w_i}{A_i}} \tag{10}$$

$$\sigma_e = \frac{1}{N} \sum i\left(\frac{\mu}{\rho}\right)_i \frac{f_i A_i}{Z_i} \tag{11}$$

where N_A, A_i, f_i, and Z_i represent the Avogadro constant, the atomic weight of the element, the fractional abundance, and the atomic number of the target element.

The effective atomic number (Z_{eff}), which identifies photon interaction in terms of photoelectric absorption and Compton scatter, can be estimated from the total atom cross section and total electronic cross section using the following relation [21]:

$$Z_{eff} = \frac{\sigma_a}{\sigma_e} \tag{12}$$

The number of electrons per unit mass of the shielding material and the electron density can be calculated using the following relationship [21]:

$$N_{eff} = N \frac{Z_{eff}}{\sum i f_i A_i} \tag{13}$$

The mean free path (MFP), which indicates the average distance that the photon is able to travel through the barrier, is inversely proportional to the linear attenuation coefficient, LAC. The MPF can be estimated using the following equation [22–25]:

$$\mathrm{MFP} = \frac{1}{\mathrm{LAC}(\mu)} \tag{14}$$

The necessary thickness of the shielding material, which is characterized by the half-value layer (HVL) and the tenth value layer (TVL), is inversely proportional to the LAC. The following equations can be used to calculate the HVL and TVL [22–25]:

$$\mathrm{TVL} = \frac{2.302}{\mathrm{LAC}(\mu)} \tag{15}$$

$$\mathrm{HVL} = \frac{0.693}{\mathrm{LAC}(\mu)} \tag{16}$$

3. Results and Discussion

3.1. Physical and Optical Parameters

Table 1 shows the sample codes, compositions, measured densities, and refractive indices of the proposed phosphate–titanite glasses. Table 2 shows the molar volume, oxygen molar volume, oxygen packing density, energy gap, and Urbach energy of the proposed phosphate–titanite glasses. Table 3 shows the molar reflection (R_m), electronic polarizability (α_m), and metallization (M) of the studied glasses. These are the parameters that are used to determine if the current network of glasses is dense or weak. Table 1 shows that increasing the TiO_2 concentration from 2 to 6 mol percent raises the density from 2.657 to 2.682 g/cm^3. As illustrated in Table 2, the V_M and V_O of the PCKNT glass sample decreased from 39.21 to 39.101 cm^3/mol and from 15.139 to 14.867 cm^3/mol, respectively. Each variable, V_M and V_0, is exactly proportional to the spatial distribution of the oxygen in the glass matrix. Whenever the ionic radius of the modifier ion is smaller than the size of the interstices of the glass network, an attraction to oxygen ions occurs, and the size of the interstices may decrease, as reported by Shebly [26]. This leads to a decrease in the values of V_M and V_O. Otherwise, by increasing the TiO_2 content from 2 to 6 mol %, the OPD increased from 66.055 to 67.262 mol. Otherwise, upon increasing the TiO_2 content from 2 to 6 mol %, the OPD increased from 66.055 to 67.262 mol·L^{-1} due to the increased oxygen atom number per unit volume [27].

Table 2. The molar volume (V_M), oxygen molar volume (V_O), optical packing density (OPD), energy gap (Eopt), and Urbach energy (ΔE) of the prepared glasses.

Sample Code	V_M (cm^3/mol)	V_O (cm^3/mol)	OPD (mol^{-1})	Energy Gap, Eopt (eV)	Urbach Energy, ΔE (eV)
PCKNT1	37.460	14.464	69.139	3.403	0.2964
PCKNT2	37.284	14.285	70.000	3.324	0.2914
PCKNT3	37.369	14.208	70.379	3.279	0.3031

Table 3. The electronic polarizability (α_m), molar reflection (R_m), and the metallization (M) of the studied glasses.

Sample Code	Molar Polarizability, α_m, ($\mathring{A}^3$)	Molar Refraction, R_m, (cm^3 /mol)	Metallization (M) ($\pm$0.001)	Third-Order Non-Linear Susceptibility $\chi^{(3)} \times 10^{-14}$ (esu)	Nonlinear Refractive Indices, n_2, $\times 10^{-13}$ (esu)
TPNK1	5.195	13.090	0.407	4.61	6.97
TPNK2	5.310	13.383	0.402	5.44	8.22
TPNK3	5.402	13.613	0.400	5.97	9.02

The optical absorption spectra of crystal and non-crystalline materials are a useful tool for calculating optical band gap values in glass systems. As illustrated in Figure 1, appealing behavior can be observed over the wavelength range from 190 to 2500 nm. As shown in all spectra of the glasses, there is a maximal peak at the absorbance positions in the near ultraviolet range, in the wavelength range of 400–750 nm in the visible range.

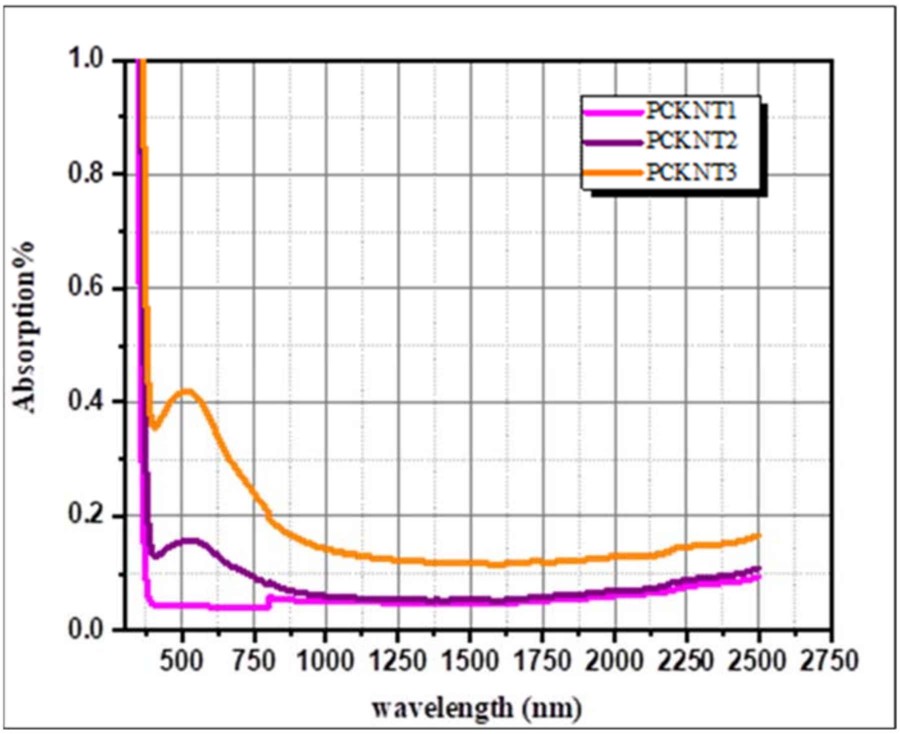

Figure 1. Absorbance spectroscopy for different compositions of PCKNT.

As shown in Figure 1, the increase in observed absorbance peaks in this range (400–600 nm) can be attribed to the increase in the TiO_2 content from 2 to 6 mol % in the prepared glass system. The observed absorbance peaks at around 497 nm indicate the presence of nanoparticle (NP) surface plasmon resonance (SPR). The SPR-related effects of the NPs of TiO_2 in the prepared glass matrices are as reported by ref. [28], showing good agreement with our results. Monge et al. [29] estimated the band that appears in the optical spectroscopy of the MgO crystals with the photon excitation of the positively charged anion vacancies at 5.0 eV is equal to the wavelength = 1.24/5 = 248 nm. Moreover, PCKNT2 and PCKNT3 have their greatest absorbance values in the visible spectrum of light, implying that they are suitable for optical applications.

The transmission spectra of the investigated glasses are depicted in Figure 2. As shown in Figure 2, the transmission spectra were calculated in the ultraviolet (UV) range through the visible (Vis) to mid-infrared (MIR) ranges.

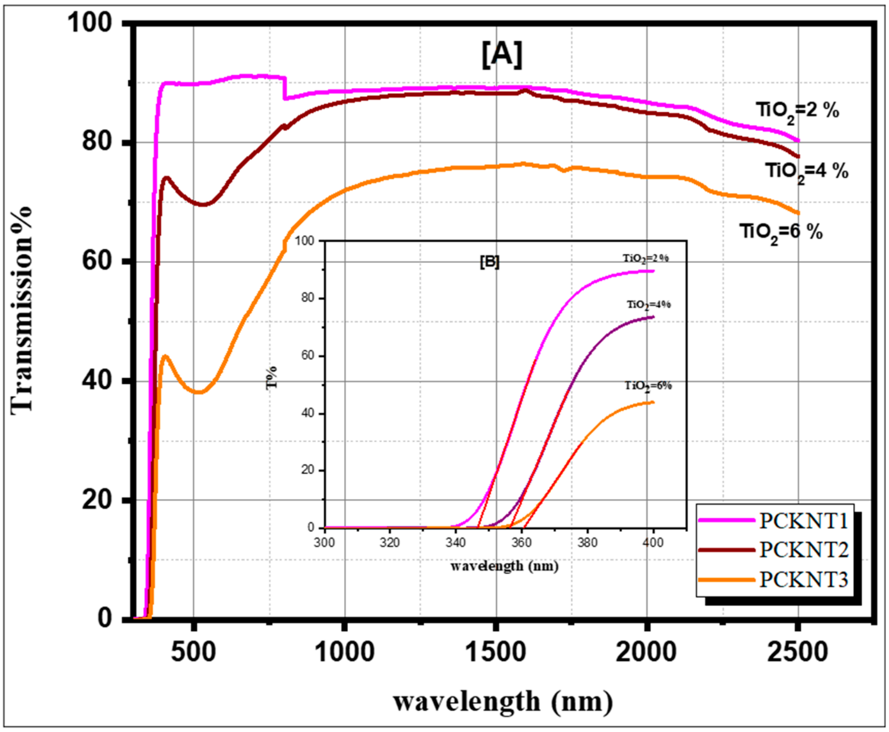

Figure 2. UV-Vis-NIR transmission spectra of the TiO_2-doped phosphate–titanite glasses.

All of the glasses are characterized by similarly shaped transmission spectra in which the MIR absorption cut-off wavelength is equal to about 563 nm. The optical absorption coefficient $\alpha(v)$ was estimated from the Beer–Lambert law (Equation (1)) using the following equation:

$$\alpha(v) = \ln(10) \cdot A/X \quad (17)$$

where A and X are the absorbance of the glass sample and the glass sample thickness, respectively. The optical band gap energy (E_{opt}) for an indirect transition can be calculated using the equation derived by Mott and Davis as follows [30]:

$$\alpha(v) = B\,(hv - E_{opt})^n/(hv) \quad (18)$$

where α, B, Hv, and E_{opt} are the absorption coefficient, constant depending on the glass composition, photon energy, and optical band energy gap, respectively.

Figure 3 shows the plot of $(\alpha kv)^{1/2}$ versus the photon energy (hv), which was used to calculate the optical energy gap for indirect transitions; the optical energy gap (E_{opt}) for glass samples was estimated by extrapolating the linear region of $(\alpha kv)^{1/2}$ vs. (hv) $(\alpha kv)^{1/2}$ = 0, as shown in Figure 3. The energy gap was found to be decreased from 3.403 to 3.279 eV when the TiO_2 concentration increased.

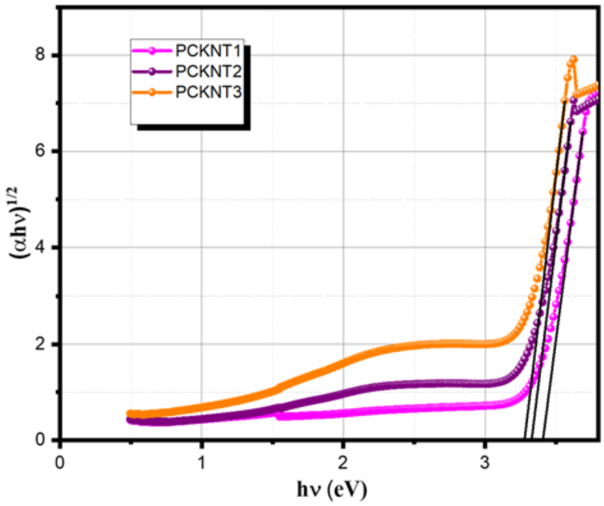

Figure 3. Plot of $(\alpha h\nu)^{1/2}$ as a function of the photon energy (hv) of prepared glasses.

The refractive index values (n) were estimated from the energy gap values using the following equation [31]:

$$\sqrt{1+\frac{E_{opt}}{20}} = \frac{(n+1)(n-1)}{n^2+2} \quad (19)$$

The value of the refractive index (n) increases from 1.616 to 1.649 when the TiO_2 concentration ranges from 2 to 6 mol %. The rise in the refractive index is due to the high polarity of the Ti^{+3} ion, which has the ability to break the bridging oxygen (BO) with low polarity and to generate non-bridging oxygen (NBO) with high polarity. The increase in the concentration of non-bridging oxygen increases the value of the refractive index, which is consistent with the findings by others [32,33]. The values of indirect E_{opt} obtained for the prepared glasses were higher than those reported in other glass systems composed of $39B_2O_3$-30PbO-20MO-$10Bi_2O_3$-$1Eu_2O_3$ (where M=K, Na, Ca, Sr, and Ba) [34], B_2O_3-CaO-TeO_2-ZnO-ZnF_2-Sm_2O_3 [35], and B_2O_3-$SrCO_3$-Nb_2O_3-$BaCO_3$-Dy_2O_3 [36]. Otherwise, the values of the density, refractive index, and optical packing density of the present glasses were lower compared to the glasses reported in Refs. [34–37].

The Urbach energy (ΔE), the width of the localized states, is utilized to measure the disorder degree of the atomic structure, which can be obtained by the following equation [33]:

$$\alpha(v) = \beta \ \exp\left(\frac{hv}{\Delta E}\right) \quad (20)$$

where (β) is constant.

Table 2 shows the Urbach energy values (ΔE). These values were estimated by taking the reciprocal of the slopes of the linear part from the plot of ln(α) against (hv), as shown in Figure 4. It was found that the value of (ΔE) increased from 0.2964 to 0.3031 eV by increasing the TiO_2 concentration from 2 to 6 mol %.

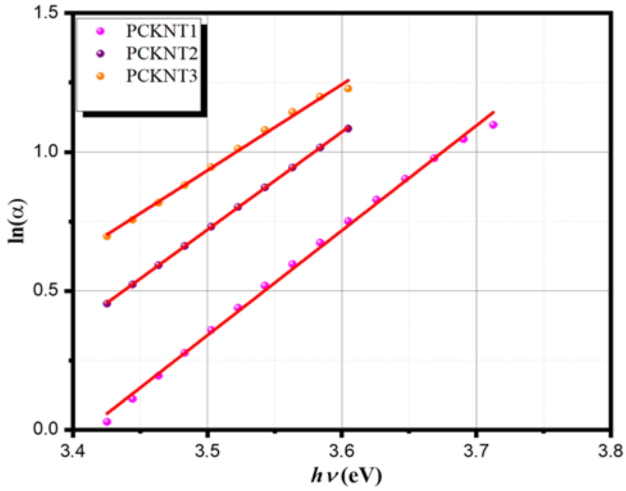

Figure 4. Plot of ln(α) as a function of the photon energy (hv) of prepared glasses.

Table 3 illustrates the molar refraction (R_m), molar polarizability (α_m), metallization (M), third-order non-linear susceptibility $\chi^{(3),}$ values and the nonlinear refractive indices, n_2. The R_m and α_m values were increased from 23.246 to 23.468 in $cm^3 \cdot mol^{-1}$ and from 9.254 to 9.313 in A^{03}, respectively, while the value M decreased from 0.407 to 0.4 as the doped TiO_2 increased from 2 to 6 mol %. The refractive index (n) value was found to be strongly dependent on the ratio α_m/V_m(i.e., the value of n increases as the ratio α_m/V_m increases). Both $\chi^{(3)}$ and n_2 increased from 4.61 to 5.97 $\times$ 10^{-14} (esu) and from 6.97 to 9.02 $\times$ 10^{-13} (esu), respectively, as the TiO_2 increased in the prepared glass matrix, which was due to the hyperpolarizability of SPR of TiO_2.

3.2. Radiation Shielding Properties

Figure 5 and Table 4 show the calculated mass and linear attenuation coefficients (MAC and LAC) for the prepared glasses at photon energies ranging between 15 keV and 200 keV using the MIKE program. As shown in Figure 5, the mass and linear attenuation coefficients show strong dependance on the photon energy. The value of the mass attenuation coefficient decreases rapidly up to a photon energy of 50 keV due to the influence of the photoelectric effect, which is the dominant interaction in low photon energies. For energies above 50 keV, the mass attenuation coefficient decreases slowly as the photon energy increases. It is clear that the reduction in the Na_2O concentration and the increase in TiO_2 result in an increase in the MAC values. The glass sample PCKNT3 has the highest MAC value among the glass samples under investigation.

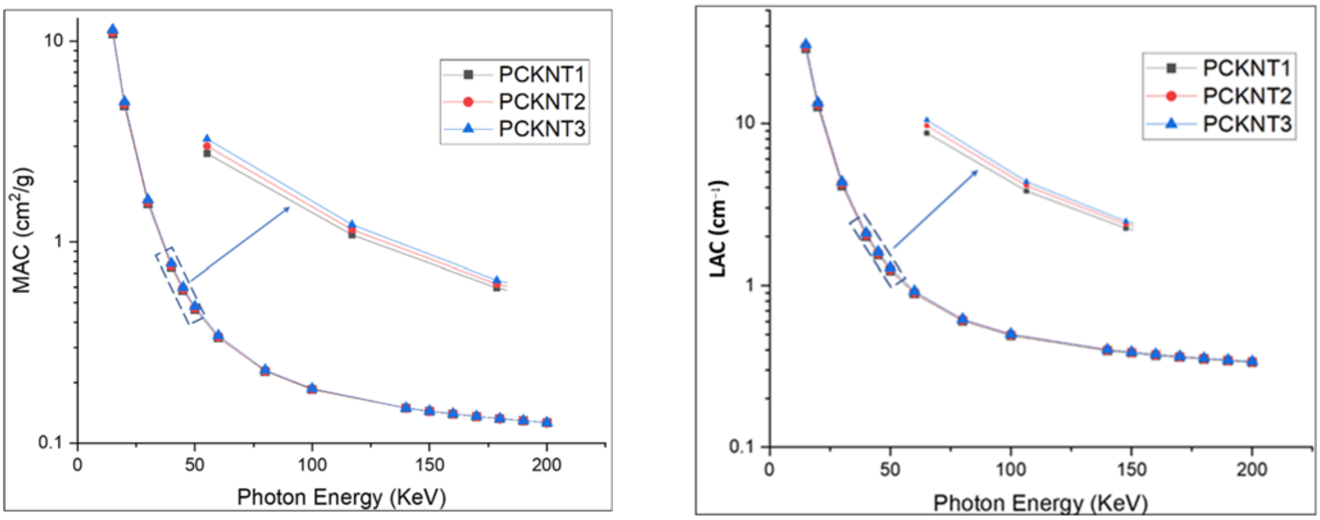

Figure 5. (**a**) The mass attenuation coefficient of prepared glasses; (**b**) the linear attenuation coefficient of prepared glasses.

Table 4. Mass and linear attenuation coefficient values for PCKNT glass systems.

Energy	MAC (cm^2/g)			LAC (cm^{-1})		
(keV)	PCKNT1	PCKNT2	PCKNT3	PCKNT1	PCKNT2	PCKNT3
15	10.90102	11.16849	11.43404	28.96401	29.92261	30.67410
20	4.774876	4.893544	5.011364	12.68685	13.11078	13.44399
30	1.548614	1.585303	1.621729	4.114668	4.247342	4.350612
40	0.751224	0.766921	0.782506	1.996003	2.054735	2.099228
45	0.576625	0.587683	0.598662	1.532093	1.574521	1.606031
50	0.464047	0.472114	0.480124	1.232974	1.264889	1.288029
60	0.334767	0.339434	0.344067	0.889477	0.909411	0.923029
80	0.227503	0.229457	0.231396	0.604476	0.614760	0.620767
100	0.184884	0.185867	0.186844	0.491237	0.497976	0.501247
140	0.149130	0.149470	0.149808	0.396238	0.400461	0.401891
150	0.143928	0.144200	0.144470	0.382417	0.386341	0.387570
160	0.139497	0.139716	0.139934	0.370643	0.374327	0.375400
170	0.135584	0.135761	0.135938	0.360247	0.363732	0.364680
180	0.132166	0.132312	0.132456	0.351165	0.354489	0.355340
190	0.129059	0.129179	0.129299	0.342910	0.346098	0.346871
200	0.126231	0.126331	0.126430	0.335397	0.338466	0.339174

The half-value layer (HVL) and mean free path (MPF) are considered important parameters used to evaluate the shielding effectiveness of the proposed material. The HVL is used to estimate the thicknesses that reduce the intensity of the radiation beam to half its initial values. They are often utilized in shielding calculations and are considered important since they quickly and directly indicate the ability of any barrier evaluated to reduce the ionizing radiation to a level that is fairly good for the environment. Table 5 and Figure 6a,b show the calculated HVL, TVL, and MFP of the prepared phosphate–titanite glasses at photon energies ranging between 15 and 200 keV. The values of HVL, TVL, and MFP decreased as the TiO_2 concentration increased. These findings are consistent with the values reported for the MAC. Furthermore, the phosphate–titanite glasses under investigation were evaluated via comparison to commercially standard shielding materials such as those developed by Schott Co., Germany (RS-253 G18, RS-520, and RS-360) [38]. As shown in Figure 7a,b, the prepared glass samples show good performance at low energies. Although the standard materials showed better shielding performance compared to the proposed phosphate–titanite, the prepared glasses have advantages as light-weighted shielding materials, especially for digital dentistry applications. In such applications, a heavy shielding material such as a lead-based shielding material is not preferable due to its toxicity and heavy weight. As shown in Figure 7a, the prepared phosphate–titanite glasses showed an HVL of less than 0.5 cm at energies up to 50 keV, which makes them the material of choice in this energy range. For instance, the values recorded for PCKNT1, PCKNT2, and PCKNT3 at 45 keV were found to be 0.443 cm, 0.432 cm, and 0.424 cm, respectively. These findings are consistent with other findings in the literature [8,9].

Table 5. Half-value layer, tenth value layer, and the mean free path of prepared PCKNT glasses.

Energy	HVL (cm)			TVL(cm)			MFP(cm)		
(keV)	PCKNT1	PCKNT2	PCKNT3	PCKNT1	PCKNT2	PCKNT3	PCKNT1	PCKNT2	PCKNT3
15	0.023926	0.023160	0.022592	0.079409	0.076865	0.074982	0.034526	0.03342	0.032601
20	0.054624	0.052857	0.051547	0.181290	0.175428	0.171080	0.078822	0.076273	0.074383
30	0.168422	0.163161	0.159288	0.558976	0.541515	0.528661	0.243033	0.235441	0.229853
40	0.347194	0.337270	0.330121	1.152303	1.119366	1.095641	0.501001	0.486681	0.476366
45	0.452322	0.440134	0.431499	1.501214	1.460762	1.432102	0.652702	0.635114	0.622653
50	0.562056	0.547874	0.538031	1.865409	1.818341	1.785674	0.811047	0.790583	0.776380
60	0.779109	0.762031	0.750789	2.585789	2.529109	2.491797	1.124256	1.099612	1.083390
80	1.146448	1.127268	1.116361	3.804949	3.741295	3.705095	1.654326	1.626650	1.610911
100	1.410726	1.391633	1.382553	4.682062	4.618695	4.588561	2.035679	2.008128	1.995026
140	1.748948	1.730506	1.724350	5.804588	5.743383	5.722951	2.523734	2.497123	2.488240
150	1.812157	1.793752	1.788063	6.014374	5.953290	5.934410	2.614945	2.588387	2.580178
160	1.869722	1.851321	1.846030	6.205428	6.144355	6.126795	2.698012	2.671459	2.663824
170	1.923683	1.905249	1.900298	6.384517	6.323339	6.306904	2.775877	2.749278	2.742132
180	1.973429	1.954925	1.950245	6.549621	6.488207	6.472675	2.847661	2.820960	2.814207
190	2.020940	2.002325	1.997862	6.707306	6.645522	6.630710	2.916220	2.889358	2.882917
200	2.066209	2.047470	2.043198	6.857546	6.795356	6.781175	2.981542	2.954503	2.948337

Table 6 and Figure 8a,b depict the Z_{eff} and N_{eff} behaviors of prepared phosphate–titanite glass samples at energies ranging between 15 and 200 keV. As shown in Figure 8, the values of Z_{eff} and N_{eff} decrease as the photon energy increases up to 200 keV. The recorded values are found to be directly correlated with the TiO_2 concentration in the glasses, following the order of PCKNT3 > PCKNT2 > PCKNT1. This was expected because the Z_{eff} and N_{eff} for all of the photons of any energy level are dependent on the mass attenuation coefficients of the constituent elements. The maximum values of Z_{eff} and N_{eff} were recorded at an energy of 15 keV. These findings are in agreement with other findings in the literature [39,40].

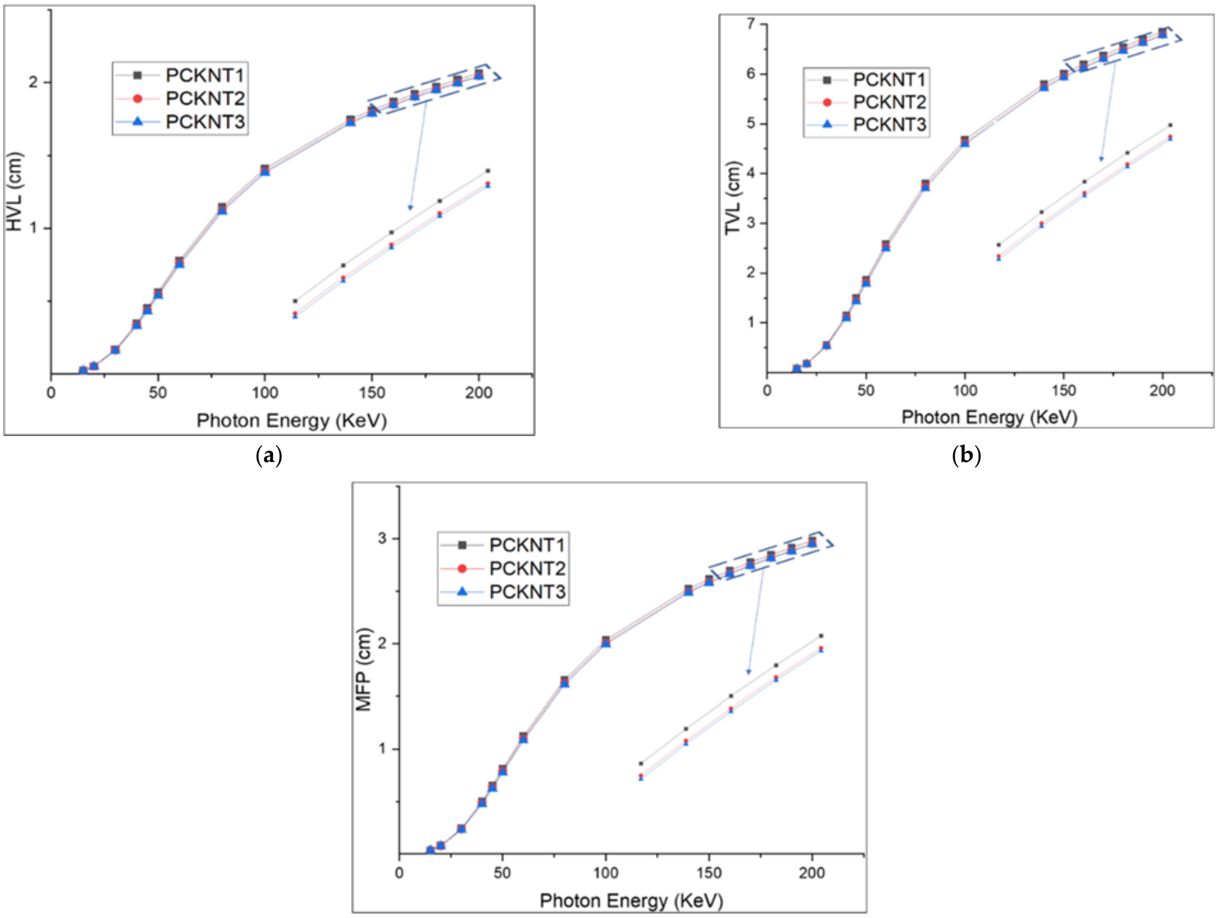

(a) (b) (c)

Figure 6. The shielding parameters of TPNK systems: (**a**) HVL, (**b**) TVL, and (**c**) MFP.

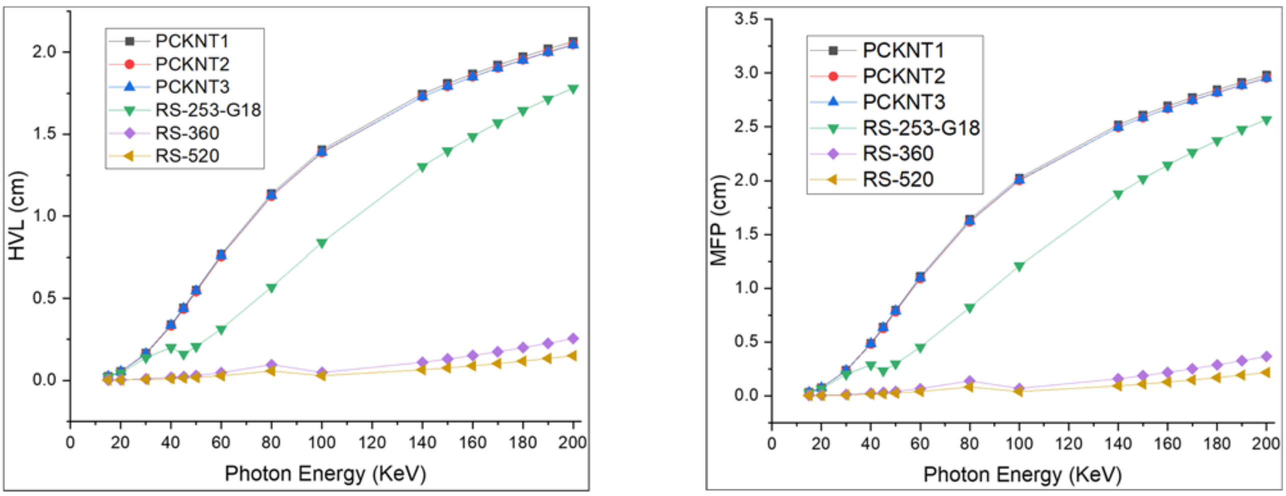

(a) (b)

Figure 7. The shielding parameters for TPNK and standard materials: (**a**) HVL and (**b**) MFP.

Table 6. Effective atomic number and effective electron density for PCKNT glasses.

Energy	Z_{eff}			$N_{eff} \times 10^{+23}$		
(keV)	PCKNT1	PCKNT2	PCKNT3	PCKNT1	PCKNT2	PCKNT3
15	15.929	16.085	16.347	4.2	4.22	4.24
20	15.850	16.008	16.273	4.18	4.21	4.22
30	15.394	15.550	15.822	4.06	4.08	4.11
40	14.696	14.842	15.117	3.88	3.90	3.92
45	14.321	14.462	14.734	3.78	3.80	3.82
50	13.958	14.090	14.357	3.69	3.71	3.73
60	13.320	13.436	13.685	3.52	3.54	3.55
80	12.447	12.534	12.747	3.29	3.30	3.31
100	11.975	12.045	12.230	3.16	3.17	3.17
140	11.566	11.618	11.775	3.05	3.05	3.06
150	11.515	11.565	11.719	3.04	3.04	3.04
160	11.474	11.522	11.673	3.03	3.03	3.03
170	11.442	11.488	11.637	3.02	3.02	3.02
180	11.415	11.460	11.606	3.01	3.01	3.01
190	11.392	11.437	11.581	2.97	2.99	3.01
200	11.375	11.418	11.561	2.95	2.97	2.99

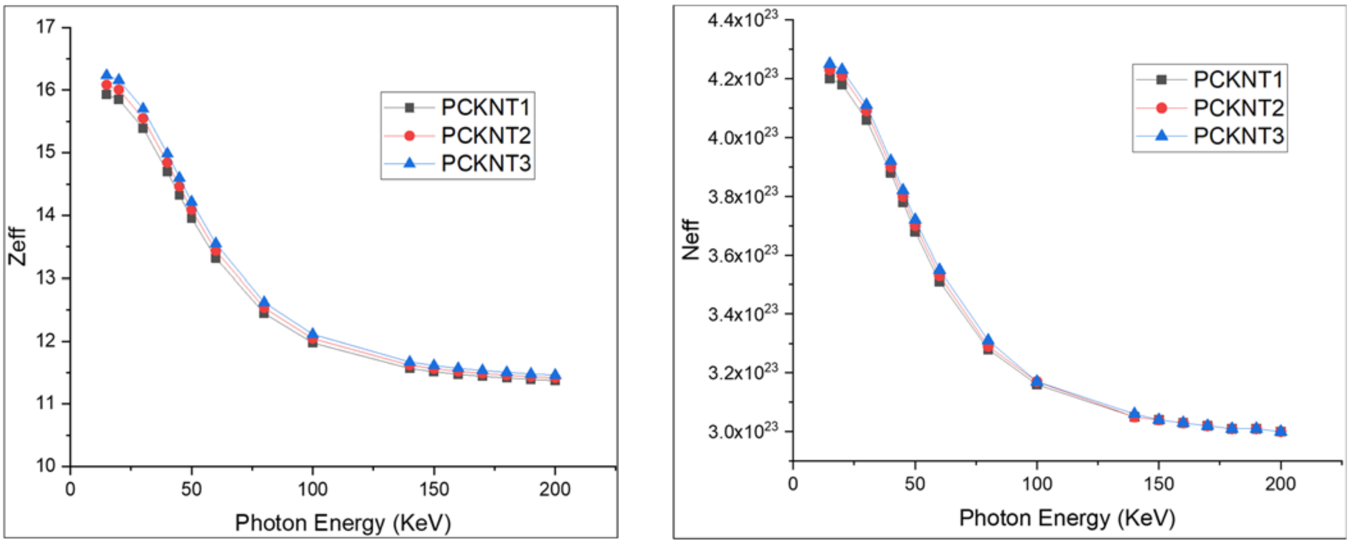

Figure 8. The radiation shielding parameters: (**a**) effective atomic number (Z_{eff}); (**b**) effective electron number (N_{eff}).

4. Conclusions

The physical, optical, and shielding properties of novel glass systems with the composition of P_2O_5-Na_2O-CaO-8KF-$CaCl_2$-xTiO_2 (where x = 2, 4, and 6) in a mol % were developed. The reported results showed that increasing the concentration of TiO_2 led to an increase in the density from 2.657 to 2.682 (g/cm^3) and an increase in the OPD from 66.055 to 67.262 mol/L, while the molar volume (V_m) and oxygen molar volume (V_0) decreased from 39.21 to 39.101cm^3/mol and from 15.139 to 14.867 cm^3/mol, respectively. The increase in both $\chi(3)$ and n_2 from 4.61 to 5.97 $\times$ 10^{-14} (esu) and from 6.97 to 9.02 $\times$ 10^{-13} (esu), respectively, when the TiO_2 in the prepared glass matrix increased, is due to the hyperpolarizability of SPR of TiO_2. Furthermore, these glasses show good shielding properties, which makes them suitable for low energy applications at the energy range between 15 and 50 keV. Further work determining the biocompatibility of the proposed materials will be conducted to study the safety and compatibility of these material for low-energy diagnostic applications.

Author Contributions: K.I.H.: conceptualization, methodology, investigation, writing—original draft, and writing—review and editing; M.S.A.: methodology, writing—review and editing, and visualization; K.J.A.: conceptualization, methodology, formal analysis, investigation, and writing—original draft; H.Y.Z.: formal analysis, review and editing, and visualization; A.M.A.: methodology, formal analysis, investigation, writing—original draft, writing—review and editing, and visualization; I.S.Y.: writing—review and editing and visualization; M.R.: methodology, formal analysis, writing—review and editing, and visualization; E.S.Y.: conceptualization, methodology, investigation, funding acquisition, writing—review and editing, and visualization. All authors have read and agreed to the published version of the manuscript.

Funding: The Deputyship for Research and Innovation, Ministry of Education, Saudi Arabia, for funding this research work through project number IFP-KKU-2020/7.

Institutional Review Board Statement: Not applicable.

Informed Consent Statement: The authors declare that they have no known competing financial interests or personal relationships that could have appeared to influence the work reported in this paper.

Data Availability Statement: Not applicable.

Acknowledgments: The authors extend their appreciation to the Deputyship for Research and Innovation, Ministry of Education, Saudi Arabia, for funding this research work through project number IFP-KKU-2020/7.

Conflicts of Interest: The authors declare no conflict of interest.

References

1. Ravindranadh, K. Bioactive glasses for technological and clinical applications. *Int. J. Chem. Sci.* **2016**, *14*, 1339–1348.
2. Vesselin, D.; Takayuki, K. Classification of Simple Oxides: A Polarizability Approach. *J. Solid-State Chem.* **2002**, *163*, 100–112. [CrossRef]
3. Larry, L.H. The story of Bioglass. *J. Mater. Sci. Mater. Med.* **2006**, *17*, 967–978.
4. Kim, J.H.; Kim, D.K.; Lee, O.J.; Ju, H.W.; Lee, J.M.; Moon, B.M.; Park, H.J.; Kim, D.W.; Lee, J.H.; Park, C.H. Osteoinductive silk fibroin/titanium dioxide/hydroxyapatite hybrid scaffold for bone tissue engineering. *Int. J. Biol. Macromol.* **2016**, *82*, 160–167. [CrossRef] [PubMed]
5. Itiravivong, P.; Promasa, A.; Laiprasert, T.; Techapongworachai, T.; Kuptniratsaikul, S.; Thanakit, V.; Heimann, R.B. Comparison of tissue reaction and osteointegration of metal implants between hydroxyapatite/Ti alloy coat: An animal experimental study. *J. Med. Assoc. Thai.* **2003**, *86* (Suppl. S2), S422–S431.
6. Awad, N.K.; Edwards, S.L.; Morsi, Y.S. A review of TiO_2 NTs on Ti metal: Electrochemical synthesis, functionalization and potential use as bone implants. *Mater. Sci. Eng. C Mater. Biol. Appl.* **2017**, *76*, 1401–1412. [CrossRef]
7. Ke, D.; Robertson, S.F.; Dernell, W.S.; Bandyopadhyay, A.; Bose, S. Effects of MgO and SiO_2 on Plasma-Sprayed Hydroxyapatite Coating: An in Vivo Study in Rat Distal Femoral Defects. *ACS Appl. Mater. Interfaces* **2017**, *9*, 25731–25737. [CrossRef]
8. Su, E.P.; Justin, D.F.; Pratt, C.R.; Sarin, V.K.; Nguyen, V.S.; Oh, S.; Jin, S. Effects of titanium nanotubes on the osseointegration, cell differentiation, mineralisation and antibacterial properties of orthopaedic implant surfaces. *Bone Jt. J.* **2018**, *100-B* (Suppl. SA1), 9–16. [CrossRef]
9. Al-Harbi, N.; Al-Hadeethi, Y.; Bakry, A.B. Mechanical and radiation shielding features of bioactive glasses: SiO_2-Na_2O-CaO-P_2O_5-B_2O_3 for utilization in dental applications. *J. Non-Cryst. Solids* **2021**, *552*, 120489. [CrossRef]
10. Alalawi, A.; Al-Buriahi, M.S.; Rammah, Y.S. Radiation shielding properties of PNCKM bioactive glasses at nuclear medicine energies. *Ceram. Int.* **2020**, *46*, 15027–15033. [CrossRef]
11. Kilicoglu, O.; Tekin, H.O. Bioactive glasses with TiO_2 additive: Behavior characterization against nuclear radiation and determination of buildup factors. *Ceram. Int.* **2020**, *46*, 10779–10787. [CrossRef]
12. Kilicoglu, O.; Tekin, H.O. Bioactive glasses and direct effect of increased K_2O additive for nuclear shielding performance: A comparative investigation. *Ceram. Int.* **2020**, *46*, 1323–1333. [CrossRef]
13. Al-Hadeethi, Y.; Al-Buriahi, M.S.; Sayyed, M.I. Bioactive glasses and the impact of Si3N4 doping on the photon attenuation up to radiotherapy energies. *Ceram. Int.* **2020**, *46*, 5306–5314. [CrossRef]
14. Tekin, H.O.; Kavaz, E.; Altunsoy, E.E.; Kilicoglu, O.; Agar, O.; Erguzel, T.T.; Sayyed, M.I. An extensive investigation on gamma-ray and neutron attenuation parameters of cobalt oxide and nickel oxide substituted bioactive glasses. *Ceram. Int.* **2019**, *45*, 9934–9949. [CrossRef]
15. Kotomin, E.A.; Popov, A.I. Radiation-induced point defects in simple oxides. *Nucl. Instrum. Methods Phys. Res. B* **1998**, *141*, 1–15. [CrossRef]
16. Girard, S.; Alessi, A.; Richard, N.; Martin-Samos, L.; de Michele, V.; Giacomazzi, L.; Agnello, S.; di Francesca, D.; Morana, A.; Winkler, B.; et al. Overview of radiation induced point defects in silica-based optical fibers. *Rev. Phys.* **2019**, *4*, 100032. [CrossRef]

17. Hussein, K.I.; Alqahtani1, M.S.; Algarni, H.; Zahran, H.; Yaha, I.S.; Grelowska, I.; Reben, M.; Yousef, E.S. MIKE: A new computational tool for investigating radiation, optical and physical properties of prototyped shielding materials. *J. Instrum.* **2021**, *16*, T07004. [CrossRef]
18. Hubbell, J.H.; Seltzer, S.M. *Tables of X-ray Mass Attenuation Coefficients and Mass Energy-Absorption Coefficients 1 keV to 20 MeV for Elements Z = 1 to 92 and 48 Additional Substances of Dosimetric Interest*; 1995-PL; National Institute of Standards and Technology: Gaithersburg, MD, USA, 1995.
19. Chilton, A.B.; Shultis, J.K.; Faw, R. *Principle of Radiation Shielding*, 1st ed.; Prentic-Halle: Englewood Cliffs, NJ, USA, 1984.
20. Kıbrıslı, O.; Ersundu, A.E.; Ersundu, M.Ç. Dy^{3+} doped tellurite glasses for solid-state lighting: An investigation through physical, thermal, structural and optical spectroscopy studies. *J. Non-Cryst. Solids* **2019**, *513*, 125–136. [CrossRef]
21. Agar, O. Study on gamma ray shielding performance of concretes doped with natural sepiolite mineral. *Radiochim. Acta* **2018**, *106*, 1009–1016. [CrossRef]
22. Tekin, H.O.; Kavaz, E.; Papachristodoulou, A.; Kamislioglu, M.; Agar, O.; Altunsoy Guclu, E.E.; Kilicoglu, O.; Sayyed, M.I. Characterization of SiO_2–PbO–CdO–Ga_2O_3 glasses for comprehensive nuclear shielding performance: Alpha, proton, gamma, neutron radiation. *Ceram. Int.* **2019**, *45*, 19206–19222. [CrossRef]
23. Mostafa, A.M.A.; Issa Shams, A.M.; Sayyed, M.I. Gamma ray shielding properties of PbO–B_2O_3–P_2O_5 doped with WO3. *J. Alloys Compd.* **2017**, *708*, 294–300. [CrossRef]
24. Rammah, Y.S.; Sayyed, M.I.; Ali, A.A.; Tekin, H.O.; El-Mallawany, R. Optical properties and gamma-shielding features of bismuth borate glasses. *Appl. Phys. A* **2018**, *124*, 83. [CrossRef]
25. Sayyed, M.I.; Kawa, M.K.; Gaikwad, D.K.; Agar, O.; Gawai, U.P.; Baki, S.O. Physical, structural, optical and gamma radiation shielding properties of borate glasses containing heavy metals (Bi_2O_3/MoO_3). *J. Non-Cryst. Solids* **2019**, *507*, 30–37. [CrossRef]
26. Kyong-Soo, H.; Miae, K.; Myoung, G.H.; Jong, P.K.; Jang, -H.Y.; Jong, H.K.; Ho-Soon, Y.; Hyun, G.K. Red-emission properties and crystallization behavior in Eu2O3-TeO2 glasses. *J. Non-Cryst. Solids* **2019**, *505*, 400–405.
27. Shelby, J.E. *Introduction to Glass Science and Technology*, 2nd ed.; The Royal Society of Chemistry: Cambridge, UK, 1997; pp. 138–161. ISBN 0-85-404639-9.
28. Kumar, A.; Gaikwad, D.K.; Obaid, S.S.; Tekin, H.O.; Agar, O.; Sayyed, M.I. Experimental studies and Monte Carlo simulations on gamma ray shielding competence of (30+x)PbO–10WO_3–10Na_2O−10MgO–(40-x)B_2O_3-glasses. *Prog. Nucl. Energy* **2020**, *119*, 103047. [CrossRef]
29. Ahmadi, F.; Ebrahimpour, Z.; Asgari, A.; Ghoshal, S.K. Insights into spectroscopic aspects of Er 3 + doped sulfophosphate glass embedded with titania nanoparticles. *Opt. Mater.* **2020**, *111*, 110650. [CrossRef]
30. Monge, M.A.; Gonzalez, R.; Munoz Santiuste, J.E.; Pareja, R.; Chen, Y.; Kotomin, E.A. Photoconversion and dynamic hole recycling process in anion vacancies in neutron-irradiated MgO crystals. *Phys. Rev. B* **1999**, *60*, 3787–3791. [CrossRef]
31. Davis, E.A.; Mott, N.F. Conduction in non-crystalline systems V. Conductivity, optical absorption and photoconductivity in amorphous semiconductors. *Philos. Mag.* **1970**, *22*, 179. [CrossRef]
32. Elkhoshkhany, N.; Reda, A.; Embaby, A.M. Preparation and study of optical, thermal, and antibacterial properties of vanadate–tellurite glass. *Ceram. Int.* **2017**, *43*, 15635–15644. [CrossRef]
33. Upender, G.; Prasad, M. Vibrational, optical and EPR studies of TeO_2-Nb_2O_5-Al_2O_3-V_2O_5glass system doped with vanadium. *Optik* **2016**, *127*, 10716–10726.
34. Divina, R.; Naseer, K.A.; Marimuthu, K.; Alajerami, Y.S.M.; Al-Buriahi, M.S. Effect of different modifier oxides on the synthesis, structural, optical, and gamma/beta shielding properties of bismuth lead borate glasses doped with europium. *J. Mater. Sci. Mater. Electron.* **2020**, *31*, 21486–21501. [CrossRef]
35. Chen, Q.; Naseer, K.A.; Marimuthu, K.; Kumar, P.S.; Miao, B.; Mahmoud, K.A.; Sayyed, M.I. Influence of modifier oxide on the structural and radiation shielding features of Sm^{3+}-doped calcium telluro-fluoroborate glass systems. *J. Aust. Ceram. Soc.* **2021**, *57*, 275–286. [CrossRef]
36. Sathiyapriya, G.; Naseer, K.A.; Marimuthu, K.; Kavaz, E.; Alalawi, A.; Al-Buriahi, M.S. Structural, optical and nuclear radiation shielding properties of strontium barium borate glasses doped with dysprosium and niobium. *J. Mater. Sci. Mater. Electron.* **2021**, *32*, 8570–8592. [CrossRef]
37. Naseer, K.A.; Marimuthu, K.; Mahmoud, K.A.; Sayyed, M.I. Impact of Bi_2O_3 modifier concentration on barium–zincborate glasses: Physical, structural, elastic, and radiation-shielding properties. *Eur. Phys. J. Plus* **2021**, *136*, 116. [CrossRef] [PubMed]
38. Hazlin, M.A.; Halimah, M.K.; Muhammad, F.D.; Faznny, M.F. Optical properties of zinc borotellurite glass doped with trivalent dysprosium ion. *Physica B* **2017**, *510*, 38–42. [CrossRef]
39. Schott Co. Radiation Shielding Glasses. Available online: https://www.schott.com/advanced_optics/english/products/optical-materials/special-materials/radiation-shielding-glasses/index.html (accessed on 24 February 2022).
40. Agar, O.; Khattari, Z.Y.; Sayyed, M.I.; Tekin, H.O.; Al-Omari, S.; Maghrabi, M.; Zaid, M.H.M.; Kityk, I.V. Evaluation of the shielding parameters of alkaline earth based phosphate glasses using MCNPX code. *Results Phys.* **2019**, *12*, 101–106. [CrossRef]